The ρ-Geminid meteoroid stream: orbits, spectroscopic data and implications for its parent body

José M. Madiedo[1,2]*

[1]*Facultad de Ciencias Experimentales, Universidad de Huelva. E-21071 Huelva, Spain*
[2]*Departamento de Física Atómica, Molecular y Nuclear, Facultad de Física, Universidad de Sevilla, E-41012 Sevilla, Spain*

ABSTRACT

By using an array of high-sensitivity CCD video devices and spectrographs, the activity of meteor events from the poorly-known ρ-Geminid meteoroid stream has been monitored during 2012 January and 2013. As a result of this research, the atmospheric trajectory and radiant position of 10 of these events has been obtained, but also the orbital parameters of the progenitor meteoroids and the tensile strength of these particles. The data reveal that the progenitor of this stream must be a comet. In addition, the emission spectra produced by three ρ-Geminid meteors were also recorded. These are the first ρ-Geminid spectra discussed in the scientific literature, and have provided clues about the chemical nature of these meteoroids and their parent body.

Key words: meteorites, meteors, meteoroids.

1 INTRODUCTION

The ρ-Geminid meteor shower was discovered by Southworth & Hawkins (1963) in the framework of the 1952–1954 Harvard Meteor Program. This poorly-known stream is currently included in the IAU working list of meteor showers with the code 94 RGE (http://www.astro.amu.edu.pl/∼jopek/MDC2007/). Its activity extends from December 28 to January 28, peaking around January 8, and its parent body remains unknown. Data about this shower are scarce (Southworth & Hawkins 1963; Lindblad 1971a,b; Sekanina 1973), mainly because of its low zenithal hourly rate (ZHR) and typical bad weather conditions in the Northern hemisphere during the above-mentioned activity period. This ZHR was of around 12 h^{-1} during the outburst exhibited on 1993 January 16 and 17 (Jenniskens 1996). In order to get a better knowledge about the ρ-Geminid meteoroid stream, additional observations of the RGE shower providing accurate enough orbital data would be necessary. With this aim, a systematic monitoring of meteor activity has been conducted in 2012 January and 2013 by using an array of high-sensitivity video devices. These devices have been proven to be very useful to obtain orbital data of meteoroids ablating in the atmosphere, and, in fact, these have become very popular in recent years (Madiedo & Trigo-Rodríguez 2008, Jenniskens et al. 2011). This paper focuses on the analysis of the multistation ρ-Geminid meteors imaged during this monitoring. Thus, atmospheric trajectories, radiant position and orbital data are presented, and several asteroids are identified as potential progenitors of this stream. In addition, three emission spectra produced by bright RGE meteors are presented and dis-

cussed. These are, to my knowledge, the first ρ-Geminid spectra discussed in the scientific literature. These spectra have provided new clues about the chemical nature of these meteoroids and their parent body.

2 INSTRUMENTATION AND METHODS

To image the ρ-Geminids discussed in this work a set of high-sensitivity CCD video devices operating at the meteor observing stations listed in Table 1 were employed. Each station operates an array of 4–12 Watec video cameras (models 902H and 902H2 Ultimate) to monitor the night sky (Madiedo & Trigo-Rodríguez 2008). These CCD video cameras generate interlaced imagery following the PAL video standard at a rate of 25 frames per second (fps) and with a resolution of 720×576 pixels. Their focal length ranges from 6 to 25 mm and the field of view covered by each device ranges, approximately, from 62° × 50° to 14° × 11°. To get an insight about the chemical nature of the progenitor meteoroids, attached holographic diffraction gratings (with 500 or 1000 lines/mm, depending on the device) were attached to the objective lens of some of these CCD cameras. These videospectrographs can record the emission spectra produced by meteor events with luminosity higher than mag –3/–4. The meteor stations work in a fully autonomous way by means of the METCONTROL software (Madiedo et al. 2010). A more detailed description of the operation of these systems is given in Madiedo & Trigo-Rodríguez (2008) and Madiedo (2014).

For data reduction, an astrometric measurement is done by hand in order to obtain the plate (x, y) coordinates of the meteor along its apparent path from each observing station. The astrometric measurements are then introduced in the AMALTHEA software (Madiedo et al. 2011), which transforms plate coordinates into equatorial

* E-mail: madiedo@cica.es

Table 1. Geographical coordinates of the meteor observing stations involved in this research.

Station #	Station name	Longitude	Latitude (N)	Alt. (m)
1	Sevilla	05° 58′ 50″ W	37° 20′ 46″	28
2	La Hita	03° 11′ 00″ W	39° 34′ 06″	674
3	Huelva	06° 56′ 11″ W	37° 15′ 10″	25
4	Sierra Nevada	03° 23′ 05″ W	37° 03′ 51″	2896
5	El Arenosillo	06° 43′ 58″ W	37° 06′ 16″	40

coordinates by using the position of reference stars appearing in the images. Typically, over 40 reference stars are used. This package employs the method of the intersection of planes to determine the position of the apparent radiant and also to reconstruct the trajectory in the atmosphere of meteors recorded from at least two different observing stations (Ceplecha 1987). The pre-atmospheric velocity V_∞ is found by measuring the velocities at the earliest part of the meteor trajectory. Once these data are known, the software computes the orbital elements of the parent meteoroid by following the method described in Ceplecha (1987).

3 OBSERVATIONS AND RESULTS

Weather conditions in Spain during 2012 January and 2013 posed important difficulties to the monitoring of the ρ-Geminids during most of its activity period. In spite of this, 21 multistation RGE meteors were imaged from the meteor observing stations listed in Table 1 from January 1 to January 18. Those events with a convergence angle below 20° were not taken into account. This is the angle between the two planes delimited by the observing stations and the meteor path in the triangulation, and it measures the quality of the determination of the atmospheric trajectory (Ceplecha 1987). By following this quality criterion 11 RGE meteors were discarded. So, as a result of the above-mentioned monitoring campaign, 10 double-station RGE meteors were considered for this research. Two of these were bright enough to produce emission spectra that were recorded by the videospectrographs. The recording dates and times of these 10 events are listed in Table 2, where their assigned SPMN codes are used for identification. The analysis of the video images provided their atmospheric trajectory, and the main parameters of these paths are also listed in Table 2 together with the position of the geocentric radiant (J2000) and the absolute magnitude of each event. The average value of the observed pre-atmospheric velocity of these particles yields $V_\infty = 22.9 \pm 0.4$ km s^{-1}. The photometric pre-atmospheric mass m_p of each meteoroid is also included in this Table. As in previous papers (see e.g. Madiedo et al. 2013d), this mass has been calculated from the light curve of each event and by using the luminous efficiency given by Ceplecha and McCrosky (1976). This mass was found to range between 0.2 and 100 g.

3.1 Orbital data

Table 3 shows the orbital elements obtained for the progenitor meteoroids of the meteor events listed in Table 2, and also the averaged orbital data calculated by taking into account these $N = 10$ orbits. In Table 3, a is the semimajor axis, e the orbital eccentricity, i the inclination, ω the argument of perihelion, Ω the longitude of the ascending node and q the perihelion distance. The values of the orbital period P and the Tisserand parameter with respect to Jupiter (T_J) are also listed. To validate the association of these events with the ρ-Geminid stream, the Southworth & Hawkins D_{SH}

Table 2. Atmospheric trajectory and radiant data (J2000) for the double-station ρ-Geminid meteors analysed in this work. M: absolute magnitude; m_p: photometric mass; H_b and H_e: beginning and ending height of the luminous phase, respectively; α_g, δ_g: right ascension and declination of the geocentric radiant; V_∞, V_g, V_h: observed pre-atmospheric, geocentric and heliocentric velocities, respectively.

Meteor code	Date and Time (UTC) ±0.1s	M ±0.5	m_p	H_b (km)	H_e (km)	α_g (°)	δ_g (°)	V_∞ (km s^{-1})	V_g (km s^{-1})	V_h (km s^{-1})
030112	2012 Jan. 3 2h24m52.8s	−4.5	15±2	92.6	60.0	98.68±0.16	33.46±0.07	23.5±0.5	20.9±0.5	38.1±0.5
060112	2012 Jan. 6 0h35m16.9s	−3.0	6.6±0.6	94.5	53.1	97.98±0.10	28.76±0.05	22.8±0.3	20.0±0.3	38.5±0.3
050113	2013 Jan. 5 23h31m38.1s	0.0	0.2±0.02	91.8	78.5	101.47±0.11	27.42±0.08	23.3±0.4	20.4±0.4	38.1±0.4
070113a	2013 Jan. 7 2h48m06.1s	−6.0	100±10	96.3	55.2	101.10±0.53	30.90±0.06	22.5±0.5	19.8±0.6	38.2±0.5
070113b	2013 Jan. 7 23h03m08.9s	−1.5	3.5±0.3	89.8	51.2	102.09±0.06	28.03±0.06	23.0±0.3	20.1±0.3	38.3±0.3
090113	2013 Jan. 9 18h41m04.2s	−2.0	4.3±0.3	94.0	62.5	102.60±0.36	31.89±0.33	22.7±0.4	19.5±0.4	38.4±0.4
110113	2013 Jan. 11 23h56m01.3s	−1.5	3.0±0.4	90.6	64.1	109.11±0.46	31.51±0.07	23.6±0.4	20.8±0.5	38.2±0.4
120113	2013 Jan. 11 0h08m46.3s	−0.5	1.3±0.2	93.2	72.5	104.82±0.04	27.46±0.03	22.2±0.4	19.2±0.5	38.2±0.4
130113	2013 Jan. 13 23h09m59.9s	−5.5	65±6	92.3	<67.3	111.15±0.04	30.61±0.02	23.6±0.5	20.8±0.5	38.3±0.5
180113	2013 Jan. 18 22h58m05.2s	−3.0	7.8±0.7	90.3	55.3	112.12±0.08	31.18±0.03	22.1±0.3	19.1±0.3	38.3±0.3

Table 3. Orbital elements (J2000) for the double-station ρ-Geminid meteors discussed in the text, and value of the D_{SH} dissimilarity function. The averaged orbit (for $N = 10$ meteors) is also included.

| Meteor code	a (au)	e	i (º)	Ω (º) $\pm 10^{-5}$	ω (º)	q (au)	P (yr)	T_J	D_{SH}
030112	2.55±0.20	0.746±0.020	6.6±0.2	281.94757	258.56±0.24	0.646±0.006	4.07	2.96±0.10	0.10
060112	2.75±0.14	0.753±0.013	3.3±0.1	284.94058	253.39±0.16	0.681±0.003	4.58	2.85±0.08	0.12
050113	2.52±0.15	0.741±0.017	2.8±0.1	285.66103	257.85±0.17	0.652±0.004	4.00	2.99±0.09	0.06
070113a	2.56±0.19	0.734±0.022	4.7±0.2	286.80531	254.30±0.79	0.679±0.007	4.10	2.98±0.12	0.10
070113b	2.64±0.13	0.745±0.013	3.1±0.1	287.67550	257.07±0.09	0.671±0.003	4.29	2.92±0.06	0.07
090113	2.67±0.20	0.739±0.021	5.2±0.2	289.51575	251.53±0.52	0.697±0.004	4.37	2.90±0.10	0.11
110113	2.61±0.18	0.750±0.018	5.8±0.1	291.77423	257.38±0.69	0.653±0.005	4.23	2.91±0.09	0.08
120113	2.57±0.16	0.730±0.018	2.7±0.1	291.80112	252.13±0.06	0.695±0.004	4.14	2.96±0.09	0.09
130113	2.62±0.21	0.750±0.022	5.4±0.1	293.78014	257.26±0.04	0.654±0.005	4.24	2.90±0.10	0.09
180113	2.67±0.13	0.733±0.014	5.2±0.1	298.86338	249.59±0.11	0.712±0.003	4.38	2.90±0.08	0.12
Average	2.62±0.15	0.742±0.016	4.7±0.1	289.27646	254.71±0.29	0.674±0.004	4.24	2.93±0.10	0.07
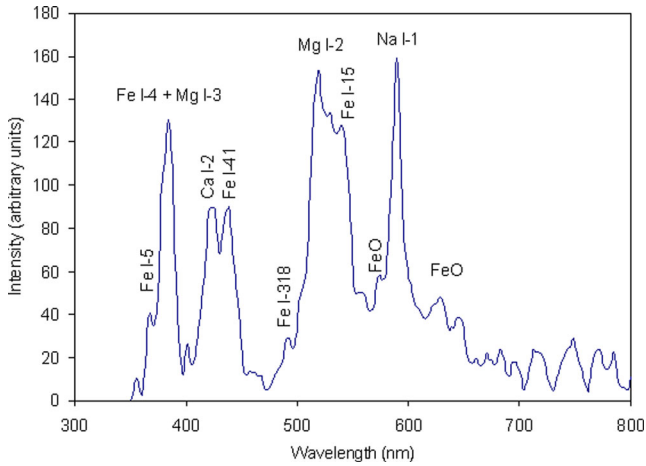
Figure 1. Calibrated emission spectrum integrated along the atmospheric trajectory of the 130113 meteor, where the main lines identified in the signal have been highlighted.

dissimilarity function (Southworth & Hawkins 1963) was calculated. As Table 2 shows, D_{SH} values obtained by comparing the orbit of this stream (Lindblad 1971a, Jenniskens 2006) with the orbits of these meteoroids remain below the usual cut-off value of 0.15 adopted to establish a valid link (Lindblad 1971a,b).

3.2 Emission spectra

The emission spectra of three ρ-Geminid fireballs (events with SPMN code 060112, 130113 and 180113 in Table 2) were imaged by the videospectrographs. However, those of meteors SPMN060112 and SPMN180113 were of very limited use, since the signal was not bright enough to show contributions other than the corresponding to the Na doublet at 588.9 nm and the Mg triplet at 516.7 nm. Fortunately, the third spectrum, which was produced by event SPMN130113, showed much more contributions. These spectra were reduced by following the standard procedure described in Madiedo et al. (2013c). Thus, the video files containing these signals were deinterlaced, sky-background-subtracted and flat-fielded. Next, each spectrum was calibrated in wavelength by using typical metal lines appearing in meteor spectra, and then corrected by taking into account the instrumental efficiency of the recording device.

The calibrated spectrum of fireball SPMN130113 is shown in Fig. 1, where the most important contributions have been highlighted and multiplet numbers are given according to Moore (1945).

The most significant contributions correspond to the Mg I-2 triplet at 516.7 nm and the Na I-1 doublet at 588.9 nm. The emission from Ca I-2 (422.6 nm), Fe I-41 (441.5 nm) and Fe I-15 (526.9 nm) are also very noticeable, together with the signal from Fe I-4 (385.6 nm) and Fe I-3 (383.8 nm), although these two are not individually resolved. In addition, the emission from FeO was identified around the Na I-1 line.

4 DISCUSSION

4.1 Meteoroid strength

According to Ceplecha (1988), meteoroids can be classified into four different populations or groups on the basis of the so-called K_B parameter. This parameter is given by the following equation:

$$K_B = \log \rho_B + 2.5 \log V_\infty - 0.5 \log \cos z_R + 0.15, \qquad (1)$$

where ρ_B is the air density at the beginning of the luminous trajectory (in g cm^{-3}), V_∞ is the pre-atmospheric velocity of the meteoroid (in cm s^{-1}) and z_R is the inclination of the atmospheric trajectory with respect to the vertical. Thus, depending on the value of K_B, meteoroids can belong to any of the following groups: A-group, comprising particles similar to carbonaceous chondrites ($7.3 \leq K_B < 8$); B-group of dense cometary material ($7.1 \leq K_B < 7.3$); C-group of regular cometary material ($6.6 \leq K_B < 7.1$) and D-group of soft cometary material ($K_B < 6.6$). In this work, the air density ρ_B in equation (1) was obtained from the US standard atmosphere model (U.S. Standard Atmosphere 1976). The calculation for the ρ-Geminids listed in Table 2 yields $K_B = 7.4 \pm 0.3$. So, within the experimental uncertainty of the data analysed here, it is not clear whether RGE meteoroids would belong to the population of dense cometary material (group B) or to the population of particles similar to carbonaceous chondrites (group A). In any event, this value of K_B suggests that these particles are tougher than regular cometary material.

The PE parameter (Ceplecha 1988), which has been traditionally employed to compare the strengths of large meteoroids, was also calculated. It is given by the following equation:

$$PE = \log \rho_E - 0.42 \log m_\infty + 1.49 \log V_\infty - 1.29 \log \cos z_R, \qquad (2)$$

where ρ_E is the air density at the terminal point of the luminous trajectory. The value of PE classifies meteoroids according to the following groups: group I, of ordinary chondritic meteoroids ($-4.6 < PE$); group II, of early type carbonaceous chondrites ($-5.25 < PE \leq -4.6$); and groups IIIa ($-5.70 < PE \leq -5.25$) and IIIb ($PE \leq -5.70$), of cometary materials. For the ρ-Geminid events analysed here, it was found that $PE = -5.02 \pm 0.31$. This result shows that it is

Table 4. Aerodynamic pressure for the flare exhibited by RGE meteors.

Meteor code	Height (km)	Velocity (km s^{-1})	Aerodynamic pressure (MPa)
030112	62.2±0.5	22.6±0.5	(1.1±0.1) × 10^{-1}
060112	61.6±0.5	21.9±0.5	(1.1±0.1) × 10^{-1}
070113a	58.2±0.5	21.2±0.5	(1.6±0.2) × 10^{-1}
070113b	56.7±0.5	21.9±0.5	(2.1±0.2) × 10^{-1}
090113	63.0±0.5	21.2±1.0	(8.8±1.3) × 10^{-2}
110113	65.0±0.5	20.2±0.5	(6.1±0.7) × 10^{-2}
180113	60.2±0.5	20.6±1.0	(1.2±0.2) × 10^{-1}

not possible to establish clearly if, from the point of view of the PE parameter, RGE meteoroids belong to the group of carbonaceous chondrites (group II) or to group IIIa of cometary materials.

The toughness of RGE meteoroids can be investigated by estimating their tensile strength. This strength can be calculated by analysing the flares exhibited by RGE meteors, as in previous papers (see e.g. Madiedo et al. 2013a). Most of the double-station ρ-Geminids in Table 2 exhibited one flare along their atmospheric path. These flares took place during the second half of their luminous trajectory. These flares occur as a consequence of the sudden fragmentation of the meteoroids in the atmosphere when the aerodynamic pressure becomes larger than the meteoroid strength. This pressure *P* is given by the following equation:

$$P = \rho_{atm} v^2, \qquad (3)$$

where *v* is the velocity of the meteoroid and ρ_{atm} the atmospheric density at the corresponding height. The flare is produced by the fast ablation of tiny fragments produced during this fragmentation, which are delivered to the thermal wave in the fireball's bow shock. According to this, the critical pressure under which the fragmentation takes place can be used as an estimation of the tensile strength of the meteoroid (Trigo-Rodriguez & Llorca 2006, 2007).

The analysis of the video images has provided the values summarized in Table 4. This shows the break-up height and velocity for each meteoroid, together with the inferred tensile strength. The atmospheric density in equation (3) was estimated again by employing the US standard atmosphere model (U.S. Standard Atmosphere 1976). These data show that the tensile strength of RGE meteoroids would range from (6.1 ± 0.7) × 10^{-2} MPa for the 110113 meteor to (2.1 ± 0.2) × 10^{-1} MPa for the 070113b event, with an average value of (1.2 ± 0.1) × 10^{-1} MPa. These value are higher than the average strength inferred for meteoroids belonging to old stream, such as the Taurids (~3.4 × 10^{-2} MPa) and the Quadrantids (~2 × 10^{-2} MPa) (Trigo-Rodríguez & Llorca 2006, 2007). However, they are lower than the (3.0 ± 0.3) × 10^{-1} MPa strength found for very tough Taurid meteoroids capable to penetrate very deep the atmosphere (Madiedo et al. 2014). So, the calculated strength values suggest that RGE meteoroids are composed by tough cometary materials and so their parent body must be a comet.

4.2 Beginning and ending heights

Figs 2 and 3 show the beginning and terminal heights (H_b and H_e, respectively) of meteors listed in Table 2. The only event not included in Fig. 3 is the meteor with code 130113, since its ending height was out of the field of view of both recording cameras and so it could not be measured.

The beginning height H_b of ρ-Geminid meteors was found to increase with increasing meteoroid mass. For events listed in Table 2, this height was always below 97 km above the sea level.
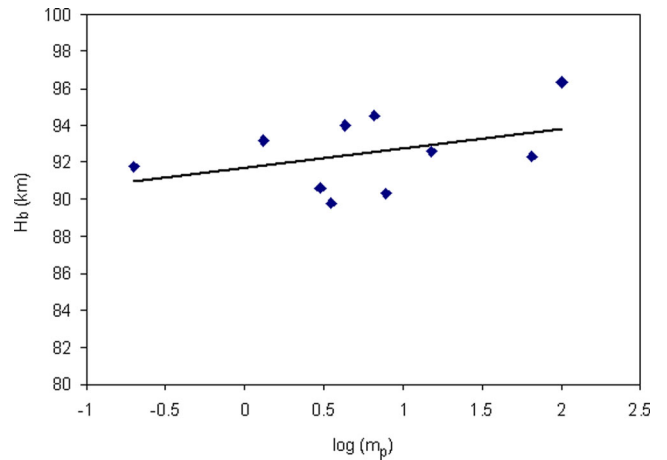
Figure 2. Meteor beginning height H_b versus logarithm of the photometric mass m_p of the meteoroid. Solid line: linear fit for measured data.
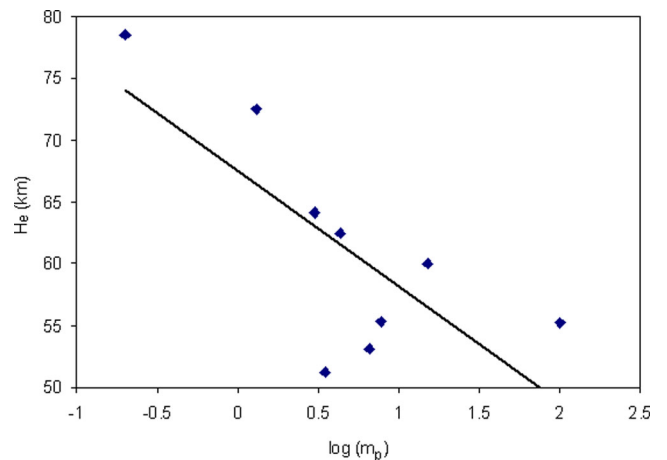
Figure 3. Meteor terminal height H_e versus logarithm of the photometric mass m_p of the meteoroid. Solid line: linear fit for measured data.

This behaviour has also been found for other cometary meteor showers, although the beginning heights exhibited by RGE meteors are lower than those exhibited by the Lyrids and the Perseids (fig. 5 in Jenniskens 2004). This can be explained on the basis of the lower pre-atmospheric velocity of the ρ-Geminids (V_∞ ~23 km s^{-1}) with respect to the Lyrids ($V_\infty = 49$ km s^{-1}) and the Perseids ($V_\infty = 61$ km s^{-1}), since the emission of radiation tends to start later for meteoroids moving at lower velocities. The dependence of H_b on the logarithm of the photometric mass was described by means of a linear relationship (solid line in Fig. 2). The slope of this straight line yields $a = 1.1 \pm 0.5$. According to this result, the increase of the beginning height with mass is less pronounced for the ρ-Geminid than for other cometary showers such as the Leonids ($a = 9.9 \pm 1.5$), the Perseids ($a = 7.9 \pm 1.3$), the Taurids ($a = 6.6 \pm 2.2$) and the Orionids ($a = 5.02 \pm 0.65$), *but more pronounced than for the Geminids (a = 0.46 ± 0.26)* (Koten et al. 2004).

Fig. 3 shows that, as expected, the terminal point of the luminous trajectory occurs at lower altitudes as the meteoroid mass increases. This behaviour can be described by means of a linear relationship between H_e and the logarithm of the photometric mass (solid line in Fig. 3), where the calculated slope of this line is $b = -9.3 \pm 0.5$. The final height of these RGE meteors is similar to the terminal level reached by the Geminids, which have an asteroidal origin (Jenniskens 2004). This does not contradict the result found in the
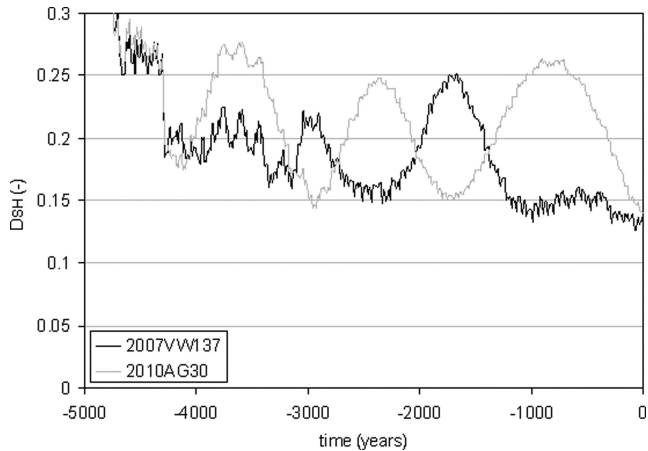
Figure 4. Evolution from present time of the D_{SH} criterion for the RGE meteoroid stream and NEOs 2007 VW137 and 2010AG30.

previous section in the sense than tensile strength values suggest that the ρ-Geminid are composed by tough cometary materials. Thus, the lower velocity of RGE meteors (about 23 km s^{-1}) with respect to the Geminids ($\sim$36 km s^{-1}) can explain that both showers exhibit a similar terminal height, since slower meteoroids tend to penetrate deeper in the atmosphere.

4.3 Orbital elements and potential parent body

The averaged value of the Tisserand parameter with respect to Jupiter yields $T_J = 2.93 \pm 0.09$. This shows that RGE meteoroids were following a Jupiter family comet orbit before impacting our planet, although this T_J value is very close to the lower limit for typical asteroidal orbits.

Orbital dissimilarity criteria were employed in order to determine the likely parent of the ρ-Geminids. These criteria are based on the calculation of the so-called dissimilarity function, which measured the 'distance' between the orbits of the parent candidate and the meteoroid stream. A review about this topic can be found in Williams (2011). According to this approach, a parent body would be associated to a given meteoroid stream if the value of the dissimilarity function falls below an appropriate cut-off value. Nevertheless, a positive similarity at a single time instant is not enough to claim a dynamical association, and it must be tested if this link is just casual or real (Williams 1993, 2004). Thus, the evolution with time of the dissimilarity function must be analysed in order to confirm that both orbits are similar over a period of time. Porubčan et al. (2004) studied the similarity of meteoroid orbits with their parent bodies for a period of at least 5000 years before an association is claimed, a view later supported by Trigo-Rodríguez et al. (2007). The ORAS software (Madiedo et al. 2013b) was employed to establish a potential link with one of the NEOs included in the NeoDys database (http://newton.dm.unipi.it/neodys/). This analysis has been performed by calculating the widely employed Southworth and Hawkins D_{SH} dissimilarity function (Southworth & Hawkins 1963), for which the cut-off condition $D_{SH} < 0.15$ is commonly adopted in order to validate an association (Lindblad 1971a,b). The average orbit calculated for RGE meteoroids in Table 3 has been employed for this analysis. Two NEOs have been obtained as parent candidates: 2007VW137 ($D_{SH} = 0.09$) and 2010AG30 ($D_{SH} = 0.13$). The evolution with time since the present epoch of the D_{SH} criterion for these objects and the orbit of the ρ-Geminid meteoroid stream is shown in Fig. 4. This plot shows that the similarity of
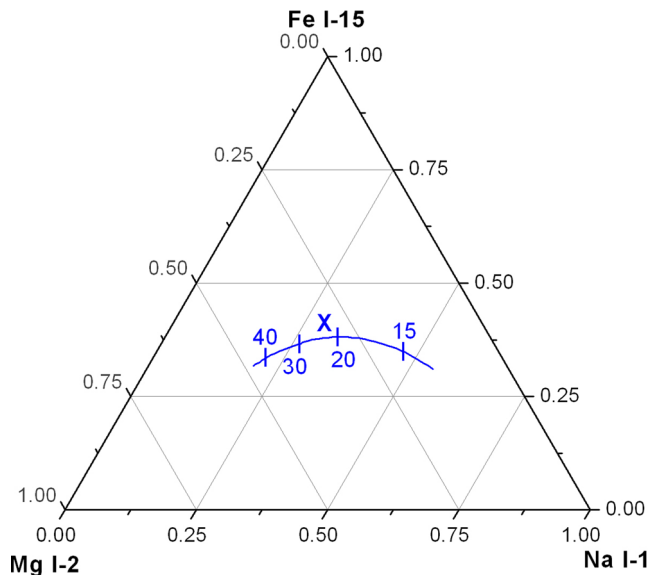

Figure 5. Expected relative intensity (solid line), as a function of meteor velocity (in km s^{-1}), of the Na I-1, Mg I-2 and Fe I-15 multiplets for chondritic meteoroids (Borovička et al. 2005). The cross shows the experimental relative intensity obtained for the 130113 meteor.

the orbits of these NEOs and the ρ-Geminids is lost within a time period of about 350 years in the past for 2007VW137, and 100 years for 2010AG30. So, it is very likely that the link found between these objects and the RGE stream is not real, but casual. As a consequence, from this analysis none of these two objects can be proposed on solid grounds as the potential parent of this stream.

4.4. Emission spectra

The SPMN130113 spectrum was studied in order to get an insight into the chemical nature of ρ-Geminid meteoroids. To do so, the emission from multiplets Na I-1, Mg I-2 and Fe I-15 has been analysed (Borovička et al. 2005). These contributions were measured frame by frame in the corresponding videospectrum, and then corrected by means of the spectral response of the recording device. For each multiplet, these contributions were then added frame by frame to obtain their integrated intensity along the atmospheric path of the fireball. Then, the Na/Mg and Fe/Mg intensity ratios were calculated. From this analysis, the ratios Na/Mg = 1.03 and Fe/Mg = 1.57 were obtained. As shown in fig. 5 in Borovička et al. (2005), the Na/Mg intensity ratios fit fairly well the result expected for meteoroids with chondritic composition for a meteor velocity of about 23 km s^{-1}. To confirm this result, the Na I-1, Mg I-2 and Fe I-15 relative intensities were plotted in the ternary diagram shown in Fig. 5, where the solid curve indicates the expected relative intensity as a function of meteor velocity for chondritic meteoroids (Borovička et al. 2005). As can be seen, the value corresponding to the SPMN130113 emission spectrum fits fairly well the expected relative intensity for a meteor velocity of about 23 km s^{-1}, which again suggests a chondritic nature for ρ-Geminid meteoroids.

With respect to the spectra of events SPMN060112 and SPMN180113, which as previously mentioned had a very limited usage, only the Na/Mg intensity ratio could be obtained since they were not bright enough to show the contributions from Fe or any other elements. The values of this intensity ratio were 1.09 and 1.01, respectively. These agree with the Na/Mg intensity ratio obtained for the SPMN130113 spectrum.

5 CONCLUSIONS

The activity of the poorly-known ρ-Geminid meteor shower was monitored and analysed in 2012 January and 2013. As a result of this survey, 10 double-station RGE meteors provided good orbits and atmospheric trajectories. The emission spectra imaged for three of these ρ-Geminid events suggest a chondritic nature for members of this meteoroid stream. Within the experimental uncertainty of the data presented here, the value obtained for the K_B parameter (7.4 $\pm$ 0.3) does not clarify whether RGE meteoroids belong to the population of dense cometary materials (group B) or to the population of particles similar to carbonaceous chondrites (group A). However, the calculated value of the Tisserand parameter shows that this meteoroid stream follows a Jupiter family comet orbit, and the tensile strength estimated for these particles is consistent with tough cometary materials. Besides, the initial height of these meteor events was found to increase as the pre-atmospheric mass of the meteoroid increases, as has been previously found for cometary meteor showers. According to this, it is concluded that the parent body of this stream is a comet. However, a search among objects currently identified in the NEO population and based on the D_{SH} Southworth and Hawking dissimilarity criterion did not allow finding any candidate as progenitor body.

ACKNOWLEDGEMENTS

REFERENCES

Borovička J., Koten P., Spurny P., Boček J., Stork R., 2005, Icarus, 174, 15
Ceplecha Z., 1987, Bull. Astron. Inst. Czech., 38, 222
Ceplecha Z., 1988, Bull. Astron. Inst. Czech., 39, 221
Ceplecha Z., McCrosky R. E., 1976, J. Geophys. Res., 81, 6257
Jenniskens P., 2004, AJ, 127, 3018
Jenniskens P., 2006, Meteor Showers and their Parent Comets. Cambridge Univ. Press, Cambridge
Jenniskens P., Gural P., Dynneson L., Grigsby B. J., Newman K. E., Borden M., Koop M., Holman D., 2011, Icarus, 216, 40
Koten P., Borovička J., Spurny P., Betlem H., Evans S., 2004, A&A, 428, 683
Lindblad B. A., 1971a, Smithsonian Contrib. Astrophys., 12, 1
Lindblad B. A., 1971b, Smithsonian Contrib. Astrophys., 12, 14
Madiedo J. M., Trigo-Rodríguez J. M., 2008, Earth Moon Planets, 102, 133
Madiedo J. M., Trigo-Rodríguez J. M., Ortiz J. L., Morales N., 2010, Adv. Astron., 2010, 1
Madiedo J. M., Trigo-Rodríguez J. M., Lyytinen E., 2011, in Cooke W. J., Moser D. E., Hardin B. F., Janches D., eds, Proc. Meteoroids Conf. NASA (CP-2011-216469), Meteoroids: The Smallest Solar System Bodies. NASA, Washington, DC, p. 330
Madiedo J. M., 2014, Earth, Planets Space, 66, 70
Madiedo J. M. et al., 2013a, MNRAS, 431, 1678
Madiedo J. M., Trigo-Rodríguez J. M., Williams I. P., Ortiz J. L., Cabrera J., 2013b, MNRAS, 431, 2464
Madiedo J. M. et al., 2013c, MNRAS, 433, 571
Madiedo J. M. et al., 2013d, A&A, 555, A149
Madiedo J. M. et al., 2014, Icarus, 231, 356
Moore C. E., 1945. A Multiplet Table of Astrophysical Interest. Princeton Univ. Obser., Princeton, NJ. Contribution No. 20
Porubčan V., Williams I. P., Kornoš L., 2004, Earth, Moon Planets, 95, 697
Sekanina Z., 1973, Icarus, 18, 253
Southworth R. B., Hawkins G. S., 1963, Smithsonian Contrib. Astrophys., 7, 261
Trigo-Rodríguez J. M., Llorca J., 2006, MNRAS, 372, 655
Trigo-Rodríguez J. M., Llorca J., 2007, MNRAS, 375, 415
Trigo-Rodríguez J. M. et al., 2007, MNRAS, 382, 1933
U.S. Standard Atmosphere, 1976, NOA-NASA-USAF, Washington, DC
Williams I. P., 2011, A&G, 52, 20
Williams I. P., Wu Z. D., 1993, MNRAS, 262, 231
Williams I. P., Ryabova G. O., Baturin A. P., Chernitsov A. M., 2004, MNRAS, 355, 1171

This paper has been typeset from a TEX/LATEX file prepared by the author.